Original Article

JOURNAL OF REINFORCED PLASTICS & COMPOSITES

*Journal of Reinforced Plastics and Composites*
2014, Vol 33(3) 252–265

DOI: 10.1177/0731684413505787
jrp.sagepub.com

SAGE

# Mechanical and rheological response of polypropylene/boehmite nanocomposites

**D Pedrazzoli[1], F Tuba[2], VM Khumalo[3,4], A Pegoretti[1] and J Karger-Kocsis[2,4,5]**

**Abstract**

In this study, the influence of synthetic boehmite alumina nanoparticles with various surface treatments on the morphology, crystallization behavior and mechanical properties of polypropylene copolymer nanocomposites was studied. In particular, a series of polypropylene/boehmite alumina nanocomposites, containing up to 10 wt% of untreated and of octylsilane-functionalized boehmite alumina nanoparticles, were prepared by melt compounding and film blowing. A third type of composite was produced by incorporation of boehmite alumina nanoparticles treated with benzene sulfonic acid. Scanning electron microscopy indicated that boehmite alumina nanoparticles were finely and uniformly dispersed, though agglomerated, in the polypropylene nanocomposites. Surface-treated boehmite alumina nanoparticles were better dispersed in the matrix than the untreated boehmite alumina nanocomposites. The melt viscosity of nanocomposites remained unaltered or decreased by nanofiller incorporation at low concentration (2.5 and 5 wt%), while it slightly increased at higher concentrations (10 wt%). Uniaxial tensile tests indicated that the nanoparticles can induce a remarkable stiffening effect even at a rather low filler content, especially in the case of surface-treated particles. The plane stress fracture toughness of the material, evaluated by the essential work of fracture approach, showed a noticeable improvement due to boehmite alumina incorporation, with an optimal effect for a filler concentration of about 2.5 wt%.

**Keywords**

Nanocomposite, polypropylene, boehmite, rheology, creep, essential work of fracture, tensile properties

## Introduction

Nanocomposites formed by incorporating organic or inorganic nanofillers in a polymeric matrix are a relatively new class of composite materials. The introduction of nanodispersed particles in low quantities (i.e. less than 5–10 wt%) can remarkably increase the performances of conventional polymeric matrices.[1–3] Improvements in the thermal, mechanical, rheological and morphological properties can occur simultaneously.[2,4] Furthermore, novel and specific functionalities, such as increased chemical and flame resistance, improved electrical conductivity, barrier properties, dimensional stability and optical homogeneity,[5] can be added. Interfacial interactions and dispersion level of fillers are key issues in determining the final performance of polymer nanocomposites.[6,7]

Isotactic polypropylene (PP) is probably one of the most interesting commodity thermoplastics that is widely used in many fields such as automotive, construction and home appliances. In particular, PP is extensively utilized not only because of its balanced thermal and mechanical properties but also because of its environmental friendliness and easy processability at a relatively low cost.[8] PP has also been widely used in

[1]Department of Industrial Engineering and INSTM Research Unit, University of Trento, Via Mesiano 77, Trento, Italy
[2]Faculty of Mechanical Engineering, Department of Polymer Engineering, Budapest University of Technology and Economics, Budapest, Hungary
[3]Polymers and Composites, Materials Science and Manufacturing, Council for Scientific and Industrial Research (CSIR), Pretoria, South Africa
[4]Department of Polymer Technology, Faculty of Mechanical Engineering and Built Environment, Tshwane University of Technology, Pretoria, South Africa
[5]MTA–BME Research Group for Composite Science and Technology, Mű egyetem rkp 3, Budapest, Hungary

**Corresponding author:**
A Pegoretti, Department of Industrial Engineering and INSTM Research Unit, University of Trento, Via Mesiano 77, 38123 Trento, Italy.
Email: alessandro.pegoretti@unitn.it

association with various types of nanofillers, such as carbon nanotubes and nanofibre,[9–11] layered silicates[12–14] and graphites,[15–17] nanoparticles such as silica[2,18] and calcium carbonate.[19,20] An important role is played by such inorganic nanofillers, which can be usually dispersed at nanometric level without the addition of compatibilizers. Metal oxides, such as ZnO, $MgO_2$, $Al_2O$, and so forth, in their nanocrystalline forms, have been found to have unique properties when compared with their respective microcrystalline form.[21] Among inorganic nanofillers, boehmite alumina (BA), with chemical formula n-AlO(OH), represents an ideal candidate because of its economic and relative easy production process.[22] BA has recently become the subject of research attention as a new type of additive for enhancing the mechanical, thermal and fire-retardant performance of polymers. Streller et al.[23] reported on how the addition of these highly dispersible particles produced significant improvements in the mechanical properties of PP. The incorporation of up to 8 wt% of BA nanoparticles has been proven to induce a remarkable reinforcement of low-density polyethylene (LDPE) and to also improve the ductility of high-density polyethylene (HDPE).[24,25] Halbach and co-workers[26,27] studied the effect of BA addition on the mechanical behavior and morphology of HDPE and poly(ethylene-co-1-octene) thermoplastic elastomers. In particular, different BAs with various sizes, shapes and aspect ratios were considered, showing that stiffness of HDPE improved upon nanofiller addition without negative effects on the elongation-at-break. In fact, the increase in stiffness was accompanied by a simultaneous increase of the elongation-at-break. Özdilek et al.[22,28] and Tuba et al.[29]studied the effects of both untreated and surface-treated BA on the thermo-mechanical properties and polymer morphology in polyamide 6 and polycaprolactone nanocomposites, showing that the polymer crystalline structure is significantly changed and the storage modulus is practically doubled upon inclusion of BA particles. It was also shown that both types of BA impart the thermo-oxidative stability to the polymer, with a significant increment in the heat distortion temperature. Moreover, Zhang et al.[30] showed how the thermal stability and flame-retardancy properties of polyethylene terephthalate can be enhanced significantly, following incorporation of BA nanoparticles.

Although PP does not have any polar groups in its backbone that could interact with BA nanoparticles, the latter can be adequately dispersed without surface treatment and without the use of coupling agents.

Nevertheless, some recent works showed that the organophilic surface treatment of BA particles can improve their dispersion via controlled interfacial adhesion between BA and PP.[23,31,32]

Although few reports are available in the literature examining the mechanical and structural properties of PP-BA nanocomposites,[23] no reports are available to our knowledge on a detailed investigation and comparison of untreated and surface-treated BA nanoparticles addition to PP matrices. Moreover, the study of material toughness of PP nanocomposites by applying the essential work of fracture (EWF) method still needs to be ascertained.[33,34]

Therefore, the main aim of this study is to investigate the effect of the addition of BA nanoparticles with different surface functionalizations on the morphology, thermal and mechanical properties of PP matrix. Particular attention is devoted to the study of the material toughness by the application of the EWF method.

## Experimental section

### *Materials and samples preparation*

A PP impact copolymer (MFI at 230°C and 2.16 kg = 1.5 g/10′, density = 0.905 g·cm$^{-3}$), with grade CHR 440 was provided by Sasol South Africa (Sasolburg, South Africa). As nanofiller, synthetic Disperal®80 boehmite of Sasol GmbH (Hamburg, Germany) has been used. In particular, boehmite was used in pristine (BA80) and in surface-treated forms. The latter occurred by octylsilane (BA80-OS) and by C10–C13 alkylbenzene sulfonic acid (BA80-OS2), respectively. BA was incorporated in 2.5, 5 and 10 wt%. BA80 nanoparticles were characterized and they have a crystallite size of 74.4 nm, mean particle size of 80 μm (as measured on the powder) and BET surface area of 88.0 $m^2 \cdot g^{-1}$.[24]

Samples were prepared by melt mixing using a Berstorff co-rotating twin-screw extruder (ZE-40, Berstorff, Hannover, Germany) followed by granulation. The barrel temperatures from the hoper to die were set at 185°C, 195°C, 205°C and 220°C, the screw was rotated at 100 rpm/min and the melt was passed through the extruder in ca. 80 s. The materials were successively blow molded (Scientific laboratory extruder-film blowing machine, 25 mm extruder type, model LE25-30/CV) in order to produce film sheets with a thickness of about 0.05 mm. The barrel temperatures from the hoper to die were set at 180°C, 185°C, 190°C, 195°C and 200°C, the screw was rotated at 65 rpm/min and the pressure was 21 MPa. The die temperatures were set at 200°C, 210°C and 220°C. The rolling speed of the nip rollers and pulling rollers were set at 3.1 and 3.8 m·min$^{-1}$, respectively, while the blower pressure was set at 0.4 MPa.

All specimens necessary for the mechanical tests were cut out from the films along the

machine direction. Neat matrix was denoted as PP, while nanocomposites were designated indicating the matrix and the amount and type of filler. For instance, a sample filled with 2.5 wt% of BA80-OS nanoparticles was coded as PP/2.5BA80-OS.

## Experimental techniques

*Morphology and X-ray diffraction.* Cryogenically fractured surfaces of unfilled PP and PP nanocomposites were observed at various magnifications using a Zeiss Supra 40 (Berlin, Germany) field emission scanning electron microscope at an accelerating voltage of 1 kV.

X-ray diffraction analysis was performed using the Rigaku® 3D Max X-ray diffractometer on the BA80 nanopowder and PP nanocomposites, scanning the samples in a $2\theta$ range between 3° and 67°, at a $2\theta$ step of 0.1°. The wavelength of the X-ray radiation was 0.15418 nm.

*Rheology measurements.* The melt rheology of the nanocomposites was analyzed on a Rheoplus 32 V3 dynamic oscillatory rheometer (Anton Paar Physics, Ostfildern, Germany) working under controlled strain conditions. The test geometry was a cone-plate (cone angle = 1°) with a cone diameter of 25 mm. Disk specimens of around 0.6 mm thickness were obtained by overlapping several films. By squeezing the PP disks, the gap was set at 0.5 mm. Frequency sweep tests were carried out at a temperature of 180°C. During the measurement, a small strain amplitude (1%) oscillatory shear was applied to the samples. The storage modulus, loss shear modulus ($G'$ and $G''$, respectively) and the dynamic complex viscosity $|\eta^*|$ were measured as function of angular frequency ($\omega$) in the range 0.01–100 rad/s.

*Thermal analyses.* Differential scanning calorimetry (DSC) tests were carried out using a DSC Q2000 (TA Instruments-Waters LLC, New Castle, USA) calorimeter under a constant nitrogen flow of $50\,\mathrm{ml{\cdot}min^{-1}}$. The samples were heated to 200°C, at a heating rate of $10^\circ\mathrm{C{\cdot}min^{-1}}$ with subsequent crystallization test down to 0°C setting a cooling rate of $10^\circ\mathrm{C{\cdot}min^{-1}}$. A subsequent heating scan was performed at $10^\circ\mathrm{C\,min^{-1}}$. The melting enthalpy of an ideally 100% crystalline PP has been considered as $\Delta H^0 = 209\,\mathrm{J{\cdot}g^{-1}}$.[35] Moreover, the crystallinity, $\chi_c$, of nanocomposite samples was calculated by taking the actual weight fraction of PP in the composite into account. The melting temperatures $T_{m1}$ and $T_{m2}$ were recorded during the first and second heating scans, respectively. The crystallization enthalpy $\Delta H_c$ was measured by integrating the heat flow curve during the cooling scan.

Thermogravimetric analyses (TGA) were carried out on a Q5000 IR thermogravimetric analyzer (TA Instruments-Waters LLC, New Castle, USA) by imposing a temperature ramp between 40°C and 700°C at a heating rate of $10^\circ\mathrm{C{\cdot}min^{-1}}$ under a constant nitrogen flow of $25\,\mathrm{ml{\cdot}min^{-1}}$. The onset of degradation temperature ($T_{d,\mathrm{onset}}$) was determined at the point of inflection, by drawing two tangents to the thermogravimetric curve, while the maximum rate of degradation temperature ($T_{d,\max}$) was determined from the peak maxima in the first derivative of weight loss curve (Figure 4).

*Mechanical tests.* Uniaxial tensile tests were performed on a Zwick® Z005 (Zwick GmbH, Germany) universal testing machine. According to ASTM standard D882-10, tests were performed on samples of at least five specimens of rectangular shape, with dimensions $300 \times 15 \times 0.05\,\mathrm{mm^3}$. Tests were carried out at a crosshead speed of $25\,\mathrm{mm{\cdot}min^{-1}}$, with a grip distance of 250 mm. Strain was recorded by an ME-46 Full Image Videoextensometer (Messphysik Laborgeräte GES.m.b.H., Austria), setting a gauge length of 40.0 mm, up to a maximum axial deformation of 1%. The elastic modulus was measured as the secant modulus between deformation levels of 0.05% and 0.25%, in accordance with ISO 527 standard. Uniaxial tensile properties, such as stress-at-yield ($\sigma_y$), stress-at-break ($\sigma_b$) and strain-at-break ($\varepsilon_b$), were determined at a higher crosshead speed ($500\,\mathrm{mm{\cdot}min^{-1}}$) on specimens of rectangular shape with dimensions of $100 \times 15 \times 0.05\,\mathrm{mm^3}$, setting an initial distance between the grips of 50 mm and without using the visual extensometer.

Creep and dynamic mechanical thermal analysis (DMTA) tests were performed by utilizing a dynamic mechanical analyzer DMA Q800 (TA Instruments®-Waters LLC, New Castle, USA) on rectangular specimens with dimensions of $25 \times 5 \times 0.05\,\mathrm{mm^3}$, with a gauge length of 11.5 mm. Tensile creep tests were performed under a constant stress ($\sigma_0$) of 4 MPa (i.e about 10% of the stress at yield of unfilled PP) for 3600 s at 30°C. The creep compliance $D(t)$, computed as the ratio between the strain and the creep stress, was plotted against the loading time. Creep curves were fitted in accordance with the Burgers model[36] reported in equation (1)

$$D(t) = \frac{1}{E_M} + \frac{t}{\eta_M} + \frac{1}{E_k}\left(1 - e^{\frac{E_k t}{\eta_k}}\right) \qquad (1)$$

where $E_M$ and $E_K$ are the elastic parameters, while $\eta_M$ and $\eta_K$ are parameters related to the viscous behavior of the material.

DMTA tests were performed in a temperature range between −40°C and 160°C, at a heating rate of 3°C min$^{-1}$ and a frequency of 1 Hz. A preload of 0.2 MPa and a maximum strain of 0.05% were set for each test. The most important viscoelastic functions ($E'$, $E''$, tan$\delta$) were recorded.

For the EWF tests, double-edge notched tensile (DENT) specimens, having a width ($w$) of 40 mm and a length of 80 mm (clamped length 40 mm), were used. The notches were prepared by razor blades (sliding method) and were perpendicular to the machine direction. The ligament length ($L$) was measured by a profile projector and a magnification of 15 × was used. Nominal ligament lengths of 5, 7, 9, 11, 13 and 15 mm were used (five specimens each). The thickness ($B$) of samples was measured using a Mitutoyo micrometer (accuracy: ± 0.001 mm).

The fracture tests were performed at ambient conditions (24 ± 0.5°C, RH = 40 ± 5%) using Instron 4502 (Instron, Norwood, USA) universal testing machine. The crosshead speed was set at 10 mm·min$^{-1}$, the displacement values ($x$) were calculated from crosshead travel, while the load ($F$) was recorded by employing a 100 N load cell. The validity of EWF method[33] was confirmed by

- the self-similarity of load–displacement curves
- a check on the ligament yielding – method described in the study of Tuba et al.[37]
- a lower ligament limit ($L = 5$ mm), which ensures quasi plane-stress conditions and steady-state crack propagation; determined as outlined previously[38]
- a confined plastic zone, which was ensured by the condition $L < x_p$, where $x_p$ is the estimated size of the plastic zone based on the study of Cotterell et al.[39] The other generally used criteria (i.e. $L < w/3$) seem to be too conservative; therefore $L = 15$ mm was used as the upper ligament length limit.

According to EWF approach, the total fracture work ($W_f$) can be divided in two parts: work ($W_p$) dissipated in the outer plastic zone and work ($W_e$) essential for the formation of new crack surfaces. The essential fracture work is assumed to be related to the cross-sectional area, $LB$, while the plastic work is associated with the plastic volume, $\beta L^2 B$. The EWF parameters can be estimated from the linear regression of the specific work of fracture ($w_f$) versus ligament length plots by equation (2)

$$w_f = w_e + \beta w_p L \quad (2)$$

where $w_f = W_f/\mathrm{LB}$, $w_e = W_e/\mathrm{LB}$ is the specific EWF, $w_p = W_p/L^2 B$ is the specific plastic work of fracture and $\beta$ is a geometry-dependent correction factor.

## Results and discussion

### Morphology

The morphology of the nanocomposites was examined using SEM analyses. In particular, SEM micrographs of PP containing the same amount (2.5 wt%) of BA80, BA80-OS and BA80-OS2 nanoparticles are shown in Figure 1.

Also, in the absence of a surface treatment, the shear forces developing in the melt compounder were deemed to be enough to achieve a good degree of de-agglomeration and a uniform dispersion of BA nanoparticles. In fact, nanofiller appeared to be well dispersed in PP/2.5BA80 nanocomposite, although some aggregates and agglomerates are recognizable. The dispersed nanoboehmites are organized into agglomerates with average sizes of 400–500 nm, composed of the much smaller crystallites (Figure 1(a)). Moreover, some larger humps and cavities are visible on the fractured surface, which can be traced to the rubber (ethylene-propylene) phase of the PP copolymer used.

On the other hand, the silane coupling agent present on the surface of BA80-OS nanoparticles slightly improved the filler dispersion in the polymer matrix (Figure 1(b)), leading to the presence of smaller and more uniformly distributed BA aggregates. Furthermore, a better polymer–filler adhesion occurred due to replacement of hydroxide groups on the surface of the nanoparticles with organic groups,[40] showing a lot less cavities due to detachment of aggregates and agglomerates. A similar filler dispersion is recognizable in the case of BA nanoparticles surface treated with benzene sulfonic acid (carrying apolar tails), probably because of the higher hydrophobicity of the BA, which indicates a lower tendency to filler aggregation (Figure 1(c)).[31]

The X-ray diffractograms (XRDs) of BA80 nanopowder, PP, and related nanocomposites are shown in Figure 2. XRD of BA80 nanopowder puts into evidence the presence of two main BA crystals by identification of diffraction reflections (hkl planes) at $2\theta = 14.7°$ and $2\theta = 28.4°$, typical of an orthorhombic crystalline structure.[41] The average crystallite size, calculated by the Scherrer's equation,[42] is about 72.2 nm, in accordance with the data reported on the material datasheet.[24] Although the crystallite size of the BA80-OS and BA80-OS2 nanopowders was not measured during this research, only a slight effect of the surface functionalization on the crystallite size can be assumed. In particular, a crystallite size of 38 and 40 nm was described for boehmite BA40 and BA40-OS in another report of our group.[41] According to the XRD of PP nanocomposites, the two reflections of BA (i.e. $2\theta = 14.7°$ and $2\theta = 28.4°$) are recognizable and their intensity increased with the nanofiller amount.

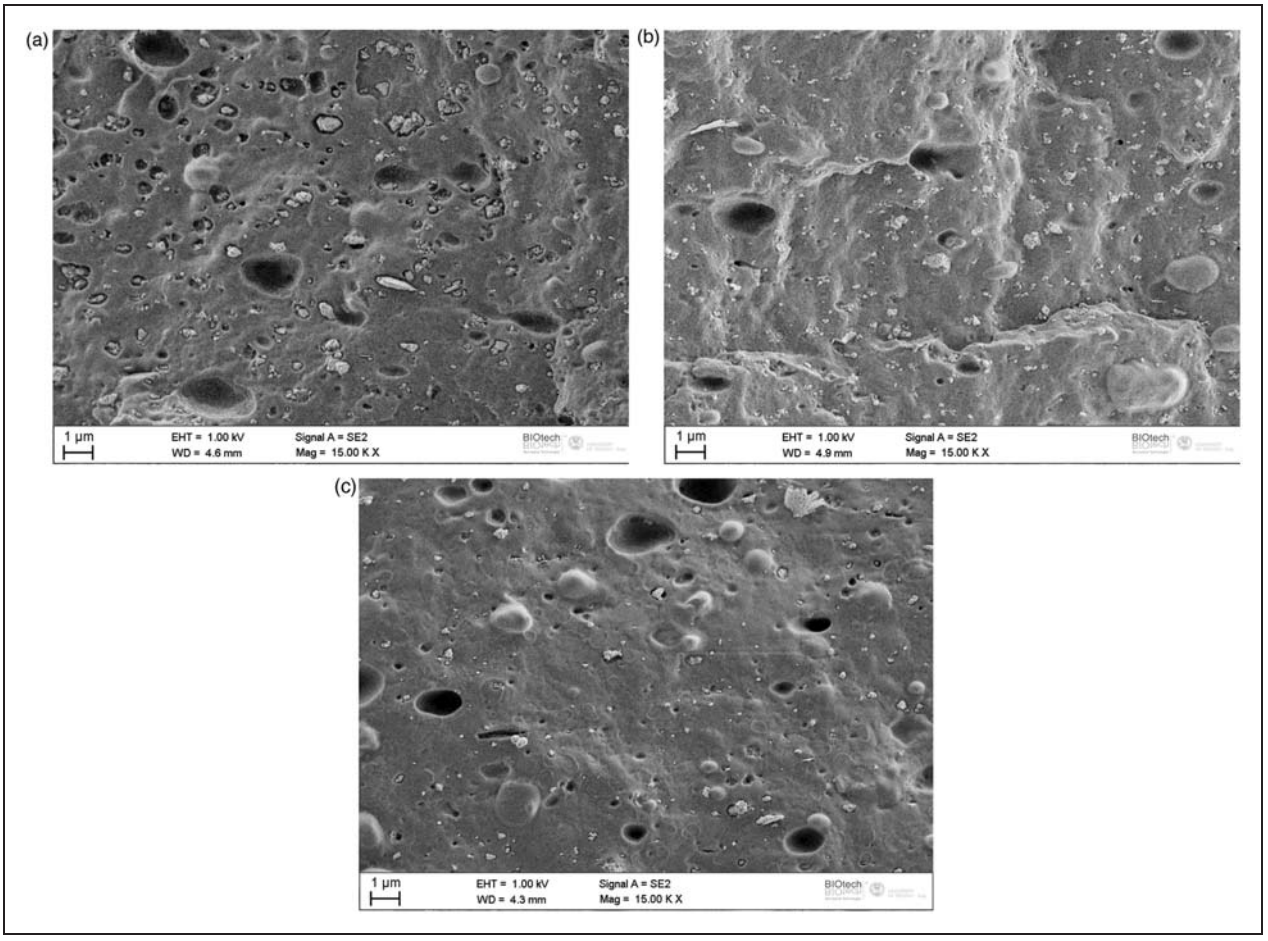


**Figure 1.** FESEM images of the fractured surface of: (a) PP/2.5BA80, (b) PP/2.5BA80-OS and (c) PP/2.5BA80-OS2 nanocomposites. FESEM: field emission scanning electron microscope; BA: boehmite alumina; PP: polypropylene.

Moreover, XRD of neat PP and its nanocomposites present the typical signals of the α-crystalline form ($2\theta = 14.0°$, $2\theta = 16.8°$, $2\theta = 18.6°$, $2\theta = 21.2°$, $2\theta = 21.8°$), while limited and sporadic occurrence of β- ($2\theta = 16.1°$) and γ- ($2\theta = 20.1°$) modifications can be observed. The diffractograms of PP nanocomposites generally indicate slightly higher matrix crystallinity when nanofillers are dispersed, in accordance with the crystallinity values measured using DSC analysis (see Table 1). In particular, the diffraction intensity of the PP peaks slightly increased after the incorporation of BA particles, although the peak at $2\theta = 16.8°$ seems to have changed without any evidence of the dependence on the filler content. The reason of this finding is not yet clear to the authors.

## *Rheological characterization*

The frequency dependence of the dynamic shear storage modulus ($G'$) and complex viscosity ($|\eta^*|$) at isothermal conditions are plotted in Figure 3(a) for neat PP and PP composites filled with 2.5 wt% of untreated and surface-treated BA nanoparticles. It is interesting to observe that $G'$ and $|\eta^*|$ values are quite similar when neat PP and nanocomposites filled with surface-treated BA nanoparticles are compared. On the other hand, a general decrease in the $G'$ and $|\eta^*|$ can be easily detected for the system modified with untreated BA over the whole frequency range. It is pertinent to note that the reduction in viscosity is certainly beneficial for the material processing. In one of our previous reports, we showed how the addition of untreated and surface-treated BA particles, with an average crystallite size of 40 nm, to a linear low-density polyethylene (LLDPE) matrix induced a decrease in $G'$ and $|\eta^*|$ compared with the unfilled LLDPE.[41] Furthermore, it was shown that a similar decrease in viscosity was obtained in the case of LLDPE systems modified with untreated BA with higher crystallite size (74 nm). Also, Blaszczak et al.[43] studied the rheological behavior of LDPE-BA nanocomposite and found that the addition of BA produced a decrease in $|\eta^*|$ when compared with the unfilled LDPE. A viscosity decrease was recorded in PP filled with untreated BA probably because the BA

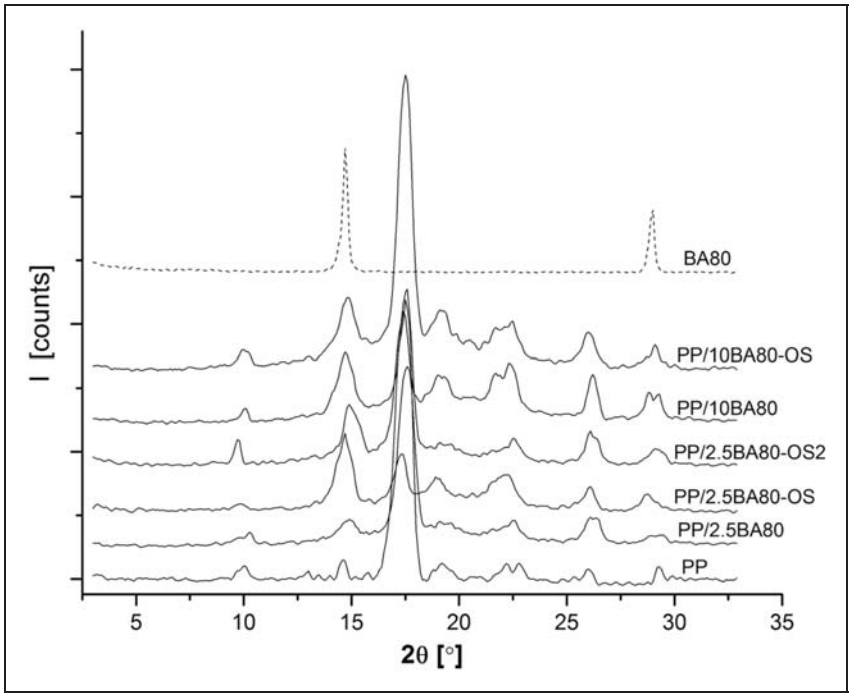


**Figure 2.** XRD of BA80 nanopowder and PP nanocomposites filled with 2.5 and 10 wt% BA. Note that the spectra of BA80-OS and BA80-OS2 should be very similar to the spectrum of BA80.
XRD: X-ray diffractogram; BA: boehmite alumina; PP: polypropylene.

**Table 1.** Melting and crystallization characteristics of unfilled PP and its nanocomposites from DSC measurements.

| Sample | $T_{m1}$ (°C) | $\Delta H_{m1}$ (J/g) ($\chi_{m1}$ (%)) | $T_c$ (°C) | $\Delta H_c$ (J/g) ($\chi_c$ (%)) | $T_{m2}$ (°C) | $\Delta H_{m2}$ (J/g) ($\chi_{m2}$ (%)) |
|---|---|---|---|---|---|---|
| PP | 162.2 | 72.3 (34.6) | 124.4 | 78.3 (37.5) | 164.3 | 77.2 (37.0) |
| PP/2.5BA80 | 163.5 | 72.9 (35.8) | 125.5 | 79.5 (39.0) | 165.0 | 77.2 (37.9) |
| PP/5BA80 | 162.6 | 73.8 (37.2) | 125.3 | 78.5 (39.5) | 164.4 | 76.0 (38.3) |
| PP/10BA80 | 163.1 | 72.8 (38.7) | 127.7 | 79.6 (42.3) | 165.0 | 76.6 (40.7) |
| PP/2.5BA80-OS | 163.3 | 73.3 (36.0) | 125.4 | 79.1 (38.8) | 165.0 | 78.7 (38.6) |
| PP/5BA80-OS | 163.0 | 73.6 (37.1) | 125.3 | 79.4 (40.0) | 164.8 | 75.7 (38.1) |
| PP/10BA80-OS | 163.4 | 73.1 (38.9) | 128.7 | 79.9 (42.5) | 165.2 | 77.4 (41.1) |
| PP/2.5BA80-OS2 | 163.8 | 73.4 (36.0) | 123.4 | 78.6 (38.6) | 164.1 | 77.1 (37.8) |

DSC: differential scanning calorimetry; BA: boehmite alumina; PP: polypropylene.

particles might have affected the chain entanglement in the melt. Furthermore, micrograph images obtained from ESEM on PP/2.5BA80-OS and PP/2.5BA80-OS2 samples show that matrix–filler adhesion was improved by the surface functionalization of BA particles. As a result of the better adhesion, the melt of filled polymer became more viscous.

Nevertheless, while similar viscosity to the unfilled PP was obtained for nanocomposites with 5 wt% BA, increases in $G'$ and $|\eta^*|$ were recorded in the case of composites filled with 10 wt% BA (Figure 3(b)). This is probably due to the nanofiller loading that was sufficiently high to allow the nanoparticles to begin to interact with each other.

Unfortunately, no result was reported regarding the PP/5BA80-OS2 and PP/10BA80-OS2 samples, as the formation of a great amount of bubbles during the film processing strongly limited the possibility of

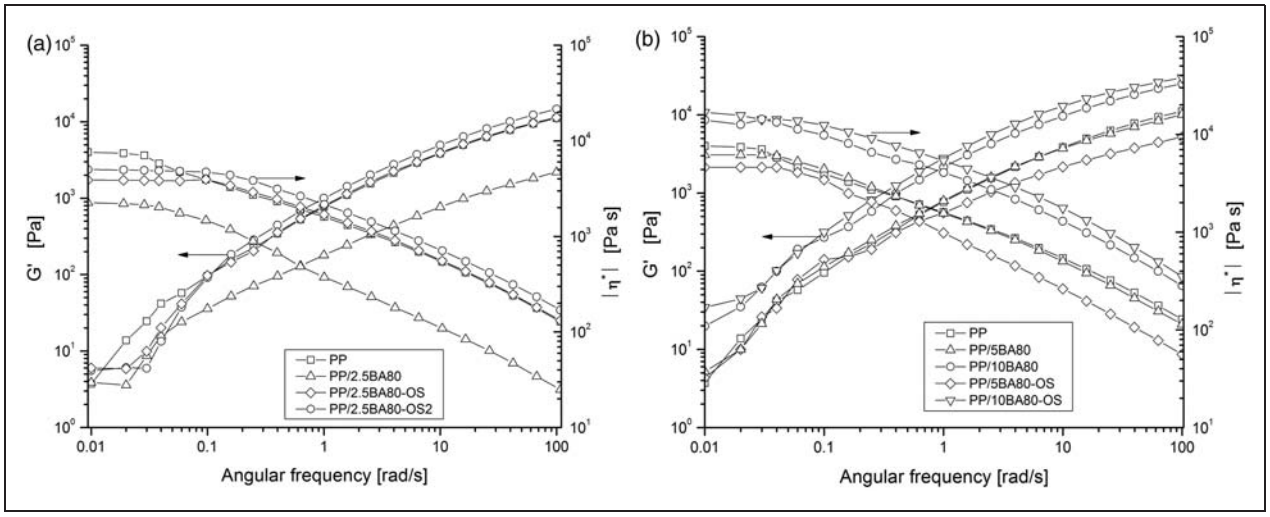


**Figure 3.** Complex viscosity $|\eta^*|$ and storage shear modulus ($G'$) with respect to angular frequency ($\omega$) for: (a) PP and PP nanocomposites filled with 2.5 wt% BA and (b) PP and PP nanocomposites filled with 5 and 10 wt% BA.
PP: polypropylene; BA: boehmite alumina.

obtaining wide specimens for rheological and mechanical testing.

## *Thermal analyses*

The most relevant parameters from DSC analysis are summarized in Table 1. It is worthwhile to observe that the addition of BA nanoparticles produced a slight increase in the crystallization peak temperature, irrespective of the boehmite type. The effect became more pronounced at 10 wt% filling. Nevertheless, no particular dependence on the filler surface treatment can be determined. The nucleating effect of BA was already reported in previous papers on LDPE and HDPE[24] and PP[23] matrices, with a different nucleating efficiency, depending on the crystallite size of the boehmite nanofiller.

While the melting temperature recorded during the second scan ($T_{m2}$) on nanocomposites was similar to that of unfilled PP, the crystallinity ($\chi_c$) increased from 37.0% to 40.7 and 41.1% after adding 10 wt% BA80 and 10 wt% BA80-OS, respectively. These results further indicate that BA may act as nucleating sites for the crystallization of PP. Streller et al.,[23] who studied the crystallization behavior of PP nanocomposites based on BA, found that the degree of crystallinity was not significantly affected by BA addition but a much larger number and higher density of spherulites was observable by means of polarization optical microscopy on molten samples when cooled down.

The thermal stability parameters as detected by TGA measurements are reported in Table 2.

**Table 2.** TGA parameters of unfilled PP and its nanocomposites.

| Sample | $T_{d,onset}$ (°C) | $T_{d,max}$ (°C) | Char (%) |
|---|---|---|---|
| PP | 441.2 | 461.8 | 0.25 |
| PP/2.5BA80 | 441.6 | 462.9 | 2.86 |
| PP/5BA80 | 445.2 | 466.1 | 4.79 |
| PP/10BA80 | 449.0 | 468.8 | 9.82 |
| PP/2.5BA80-OS | 442.5 | 463.1 | 2.90 |
| PP/5BA80-OS | 446.1 | 466.3 | 4.84 |
| PP/10BA80-OS | 449.3 | 468.7 | 9.93 |
| PP/2.5BA80-OS2 | 442.4 | 462.8 | 2.96 |

TGA: thermogravimetric analysis; PP: polypropylene; BA: boehmite alumina.

A representative thermograph of the unfilled PP, showing the thermogravimetric curve and the first derivative of weight loss curve, is reported in Figure 4. When considering PP-BA nanocomposites, $T_{d,onset}$ and $T_{d,max}$ increased with increasing filler content. This could also be attributed mainly to the dehydration process of BA nanofiller, which delayed the polymer degradation.[30] The char content at 700°C is also shown in Table 2 for all the samples. Improved thermal and thermo-oxidative stability, due to the addition of BA, has been reported for polyethylenes[24] and PP.[23,44] In one of our previous reports, a remarkable improvement in thermal resistance parameters with the incorporation of BA in LLDPE matrix was observed, indicating a slight dependence on the BA crystallite size.[41]

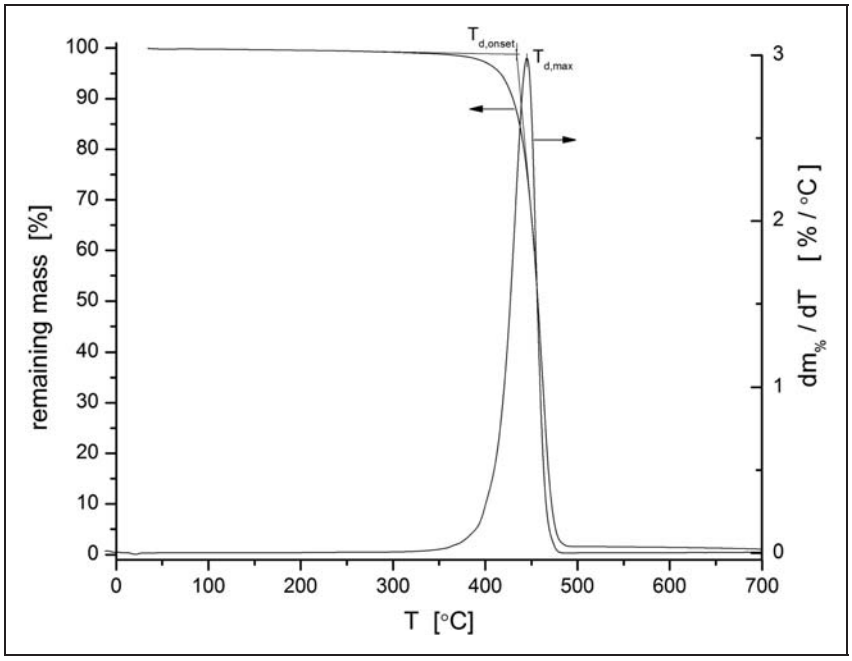


**Figure 4.** Representative thermograph of the unfilled PP, showing the thermogravimetric curve (left *y*-axis) and the first derivative of weight loss curve (right *y*-axis).
PP: polypropylene.

**Table 3.** Quasi-static tensile properties at yield and at break of unfilled PP and its nanocomposites.

| Sample | Tensile modulus (MPa) | Tensile strength at yield (MPa) | Tensile stress at break (MPa) | Elongation at break (%) |
|---|---|---|---|---|
| PP | 1426 ± 19 | 25.2 ± 0.7 | 40.0 ± 1.4 | 711 ± 32 |
| PP/2.5BA80 | 1614 ± 63 | 23.9 ± 0.6 | 28.9 ± 1.0 | 601 ± 32 |
| PP/5BA80 | 1646 ± 39 | 23.8 ± 0.7 | 23.1 ± 0.5 | 490 ± 81 |
| PP/10BA80 | 1984 ± 69 | 17.2 ± 0.5 | 17.8 ± 0.3 | 13 ± 1 |
| PP/2.5BA80-OS | 1671 ± 45 | 28.0 ± 1.4 | 31.5 ± 0.8 | 641 ± 41 |
| PP/5BA80-OS | 1712 ± 49 | 25.2 ± 0.4 | 25.6 ± 0.5 | 600 ± 66 |
| PP/10BA80-OS | 2090 ± 23 | 20.9 ± 0.5 | 20.6 ± 0.8 | 30 ± 2 |
| PP/2.5BA80-OS2 | 1644 ± 62 | 22.0 ± 0.3 | 27.5 ± 0.7 | 31 ± 4 |

BA: boehmite alumina; PP: polypropylene.

## *Mechanical testing*

The tensile modulus of PP improved by about 46% with BA content for systems filled with 10 wt% of BA80-OS (see Table 3). Moreover, the surface-treated BA nanoparticles seem to have a better efficiency in increasing the stiffness of PP with respect to untreated BA.

In general, yield stress and stress-at-break values slightly decreased with the addition of untreated BA, probably due to the filler agglomeration.[40] Interestingly, since the decrease in yield stress measured on bulk samples was accompanied by a lower viscosity of the melt polymer, BA nanoparticles might have acted as a solid-phase plasticizer.

Filler agglomeration is also supposed to be responsible for the decrease in the elongation-at-break of nanocomposites with respect to the neat matrix, showing the behavior often reported for polymer nanocomposites filled with inorganic fillers. It is worthwhile to note that the stress-at-yield, stress-at-break and strain-at-break values of PP/BA80-OS nanocomposites are higher than those of PP/BA80 at the same filler content. These results suggest that the utilization of

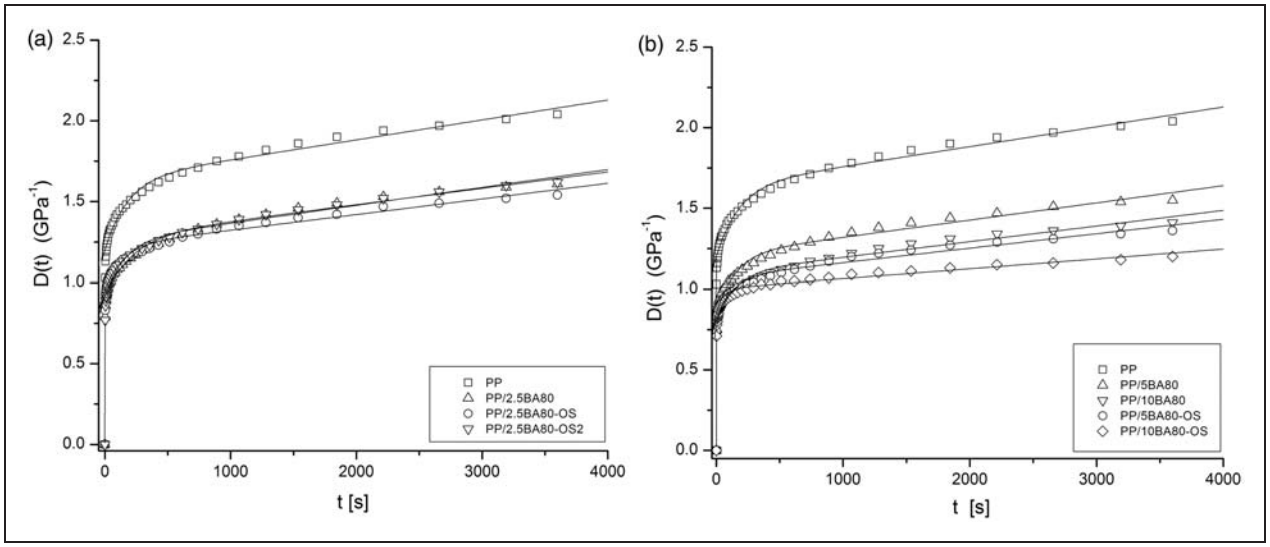


**Figure 5.** Creep compliance ($D(t)$) of neat PP and its nanocomposites ($T = 30^{\circ}C$, $\sigma_0 = 4$ MPa).
PP: polypropylene.

**Table 4.** Creep compliance data ($T = 30^{\circ}C$, $\sigma_0 = 4$ MPa) and dynamic mechanical properties of PP and its nanocomposites ($f = 1$ Hz).

| Sample | $D_e$ (GPa$^{-1}$) | $D_{ve,2000s}$ (GPa$^{-1}$) | $D_{tot,2000s}$ (GPa$^{-1}$) | $E'$ ($-40^{\circ}C$) (MPa) | $E'$ ($23^{\circ}C$) (MPa) | $E''$ ($23^{\circ}C$) (MPa) | $T_g$ ($^{\circ}C$) |
|---|---|---|---|---|---|---|---|
| PP | 1.13 | 0.79 | 1.92 | 2601.7 | 1506.1 | 70.5 | 11.6 |
| PP/2.5BA80 | 0.86 | 0.62 | 1.48 | 3020.0 | 1619.9 | 73.7 | 11.6 |
| PP/5BA80 | 0.83 | 0.63 | 1.46 | 3325.3 | 1728.9 | 74.1 | 11.7 |
| PP/10BA80 | 0.78 | 0.55 | 1.33 | 3503.6 | 2004.0 | 79.0 | 12.0 |
| PP/2.5BA80-OS | 0.91 | 0.54 | 1.45 | 3139.9 | 1737.3 | 71.2 | 11.9 |
| PP/5BA80-OS | 0.80 | 0.48 | 1.28 | 3415.2 | 1883.5 | 75.7 | 12.2 |
| PP/10BA80-OS | 0.78 | 0.36 | 1.14 | 3713.5 | 2251.7 | 87.0 | 13.3 |
| PP/2.5BA80-OS2 | 0.84 | 0.66 | 1.50 | 3204.9 | 1859.3 | 74.1 | 12.0 |

BA: boehmite alumina; PP: polypropylene.

surface-treated BA is essential to achieve higher strength and stiffness at low nanofiller concentrations. Brostow et al.[40] studied the tensile properties and properties at the interface of LDPE filled with untreated and silane-functionalized BA nanoparticles. In their study, it was shown that the strain-at-break increased with silane treatment and decreased with increment of filler loading, indicating that the silane coupling agent present on the surface of BA produced a lubricating or plasticizing effect.

Furthermore, the sample PP/2.5BA80-OS2 showed lower ultimate tensile properties (stress-at-break and strain-at-break) with respect to PP/2.5BA80 and PP/2.5BA80-OS samples. Although an increase was expected as a result of smaller agglomerations, which could act as stress concentrators for failure points, this was not the case. In particular, the remarkable decrease in the elongation at break might be attributed to the rigidity of the benzene group present on the filler surface and characterizing the polymer–matrix interface.

Figure 5(a) and (b), respectively, show the isothermal creep compliances (under a constant load of 4 MPa and at $30^{\circ}C$) of unfilled PP and PP nanocomposites filled with 2.5 wt% BA and 5 and 10 wt% BA. The elastic ($D_e$), viscoelastic ($D_{ve}$, 2000s) and total ($D_{tot}$, 2000s) components of the creep compliance after 2000 s are summarized in Table 4. The introduction of BA nanoparticles led to a significant improvement of the creep stability of the material. Moreover, the enhancement of the creep resistance of PP nanocomposites with respect to unfilled PP can be clearly detected by the higher elastic ($E_K$, $E_M$) and viscous ($\eta_K$, $\eta_M$) parameters of the Burgers model (Table 5). It is generally believed that nanoparticles can effectively

**Table 5.** Fitting parameters of creep data of PP nanocomposites in accordance with the Burgers model (equation (1)).

| Sample | $E_M$ (MPa) | $\eta_M$ (GPa s) | $E_k$ (MPa) | $\eta_k$ (GPa s) | $R^2$ |
|---|---|---|---|---|---|
| PP | $0.83 \pm 0.01$ | $8115.1 \pm 574.6$ | $2.31 \pm 0.10$ | $416.8 \pm 43.0$ | 0.990 |
| PP/2.5BA80 | $1.08 \pm 0.01$ | $9840.7 \pm 737.9$ | $2.81 \pm 0.13$ | $633.1 \pm 61.8$ | 0.990 |
| PP/5BA80 | $1.17 \pm 0.02$ | $10155.8 \pm 816.3$ | $2.88 \pm 0.15$ | $513.8 \pm 55.8$ | 0.989 |
| PP/10BA80 | $1.25 \pm 0.02$ | $10297.5 \pm 848.6$ | $3.39 \pm 0.19$ | $509.3 \pm 71.8$ | 0.990 |
| PP/2.5BA80-OS | $1.05 \pm 0.01$ | $10314.5 \pm 700.6$ | $3.69 \pm 0.19$ | $524.2 \pm 70.3$ | 0.991 |
| PP/5BA80-OS | $1.22 \pm 0.02$ | $11150.5 \pm 951.9$ | $3.98 \pm 0.25$ | $505.5 \pm 85.9$ | 0.989 |
| PP/10BA80-OS | $1.30 \pm 0.02$ | $16424.4 \pm 1318.9$ | $4.33 \pm 0.23$ | $501.2 \pm 38.9$ | 0.990 |
| PP/2.5BA80-OS2 | $1.09 \pm 0.01$ | $9027.9 \pm 516.0$ | $2.98 \pm 0.12$ | $485.4 \pm 49.4$ | 0.991 |

BA: boehmite alumina; PP: polypropylene.

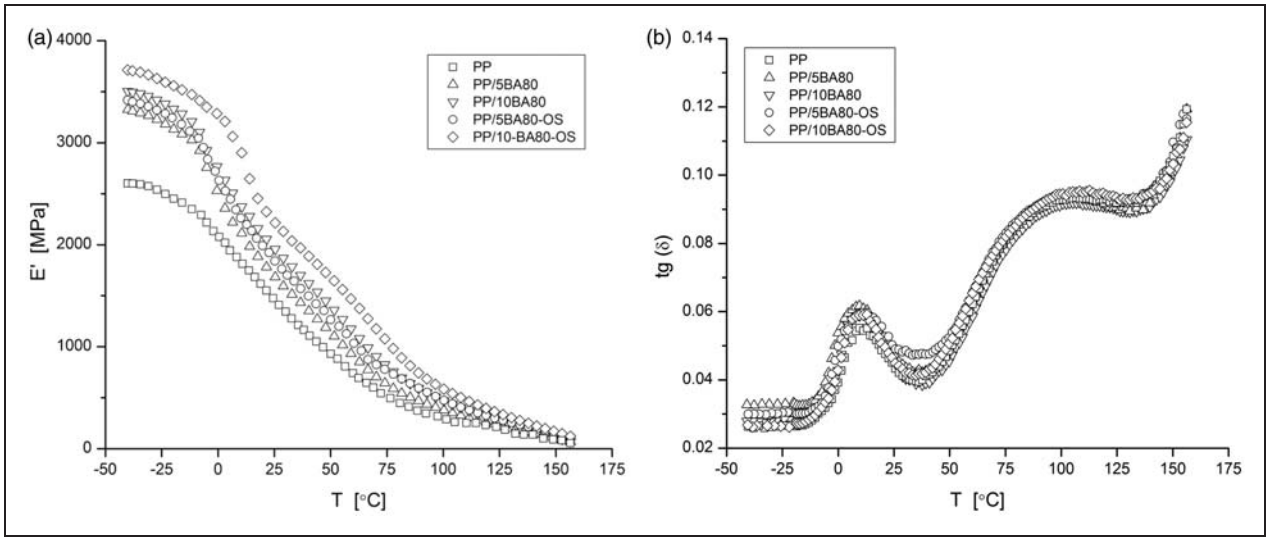


**Figure 6.** Dynamic mechanical properties of neat PP and its nanocomposites ($f = 1$ Hz): (a) storage modulus ($E'$) and (b) loss tangent (tanδ).
PP: polypropylene.

restrict the motion of polymer chains, thus influencing the stress transfer on a nanoscale, with positive effects on the creep stability of the material.[45] Although creep compliance data of nanocomposites filled with 2.5 wt% BA did not show any significant difference, the addition of BA80-OS resulted in better creep stability than BA80 at 5 and 10 wt%, showing a dependence on the BA surface functionalization. The better filler dispersion and the apolarity achieved with surface-treated BA particles not only produced higher stiffness but also promoted a more efficient stress transfer between filler and matrix, thereby strongly limiting the viscous flow.

The dynamic storage modulus ($E'$) increased remarkably with increasing BA content (Table 4), indicating that the incorporation of rigid BA nanoparticles produced a reinforcing effect. Furthermore, increase in storage modulus for the nanocomposites with surface-treated BA (i.e. PP/BA80-OS and PP/BA80-OS2) was relatively higher than that of nanocomposites containing untreated BA (i.e. PP/BA80). The results are in good agreement with the modulus improvement recorded in quasi-static tensile tests and with the improvements observed during the creep tests. Comparison plots of the storage modulus ($E'$) and loss factor (tan$\delta$), as functions of temperature, are, respectively, displayed in Figure 6(a) and (b), for unfilled PP and its nanocomposites containing 5 and 10 wt% BA. The glass transition temperature ($T_g$), as detected from the tan$\delta$ peak, slightly increased in nanocomposites of higher filler content with respect to unfilled PP, reflecting the restriction of the motion of polymer chains induced by the incorporation of nanofillers. It is well known that the $T_g$ of a polymer in a nanocomposite depends on the mobility of the chain segment of the

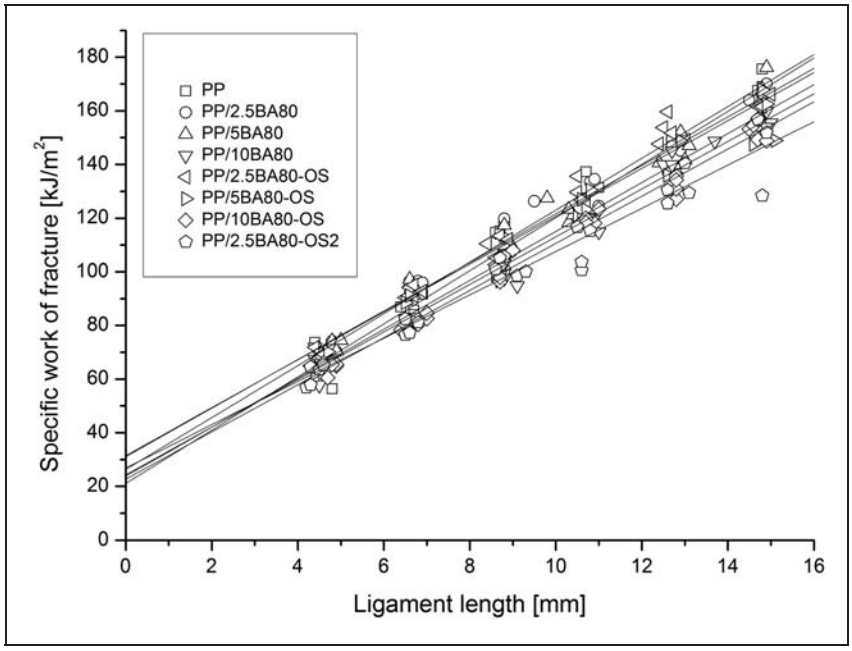


**Figure 7.** Specific work of fracture versus ligament length plots for neat PP and its nanocomposites.
PP: polypropylene.

**Table 6.** Specific EWF parameters of PP and its nanocomposites (for $w_e$ and $\beta w_p$ the 95% confidence limits are indicated).

| Sample | $w_e$ (kJ·m$^{-2}$) | $\beta w_p$ (MJ·m$^{-3}$) | $\beta$(−) | $w_p$ (MJ·m$^{-3}$) | $e_0$ (mm) | $R^2$ (−) | $N$ (−) |
|---|---|---|---|---|---|---|---|
| PP | 21.1 ± 7.3 | 9.9 ± 0.7 | 0.332 ± 0.047 | 33.1 ± 5.8 | 1.48 | 0.970 | 27 |
| PP/2.5BA80 | 31.1 ± 7.8 | 9.0 ± 0.8 | 0.275 ± 0.067 | 44.9 ± 12.3 | 1.88 | 0.963 | 25 |
| PP/5BA80 | 31.5 ± 6.8 | 8.9 ± 0.7 | 0.310 ± 0.034 | 30.7 ± 4.5 | 2.25 | 0.969 | 25 |
| PP/10BA80 | 24.4 ± 5.3 | 8.9 ± 0.5 | 0.286 ± 0.033 | 33.3 ± 4.9 | 1.49 | 0.981 | 26 |
| PP/2.5BA80-OS | 26.3 ± 5.8 | 9.7 ± 0.6 | 0.304 ± 0.044 | 35.3 ± 6.1 | 1.78 | 0.979 | 26 |
| PP/5BA80-OS | 23.8 ± 7.7 | 9.1 ± 0.7 | 0.302 ± 0.041 | 33.3 ± 5.7 | 1.54 | 0.966 | 25 |
| PP/10BA80-OS | 22.7 ± 3.9 | 8.8 ± 0.4 | 0.304 ± 0.030 | 30.3 ± 3.6 | 1.60 | 0.989 | 27 |
| PP/2.5BA80-OS2 | 24.1 ± 6.7 | 8.5 ± 0.7 | 0.321 ± 0.060 | 31.7 ± 7.0 | 1.60 | 0.967 | 24 |

BA: boehmite alumina; PP: polypropylene; EWF: essential work of fracture.

macromolecules in the polymer matrix. If the molecular chain is restricted, the motion or relaxation of the chain segment becomes difficult at the original glass transition temperature and a higher temperature is required.[46] Therefore, the increase in $T_g$ values may be related to the degree of the homogeneous dispersion of nanoparticles in the polymer matrix and the interactions between the filler and polymer.[6]

During the fracture studies, the correlation coefficients ($R^2$) of EWF tests varied between 0.96 and 0.99, while the standard deviation values scattered between 3 and 6.5 kJ·m$^{-2}$, for all samples. Based on previous studies of Williams and Rink,[47] and Tuba et al.,[48] these results are adequate for an accurate application of the EWF approach. A minimum sample size ($N$) of 25 ensured the accuracy of the measurements.[49]

The specific EWF ($w_e$) of PP increased after the incorporation of BA (Figure 7). As the crystalline morphology did not change significantly (see Table 1), this reinforcing effect can be attributed mainly to the nanofiller. Nevertheless, increasing filler content induces a reduction of $w_e$ values (Table 6), which is a general observation for the 'over-filled' nanocomposites and can be attributed to the agglomeration of nanoparticles. This disadvantageous effect caused the decrease in the yield stress (see Table 3) too. Although the OS

treatment resulted in increasing the yield stress at low filler content, the $w_e$ term did not increase further and an even more interesting observation was that it decreases. This observation is in good agreement with the observation of Arkhireyeva and Hashemi[50] regarding the direct proportion between $w_e$ and $e_0 \cdot \sigma_y$, where $e_0$ is the ordinate intercept of extension-at-break (DENT specimens) versus ligament length linear regression plots.

The nanocomposites have smaller plastic work of fracture, $\beta w_p$, values when compared with the neat PP material. The increasing filler content also resulted in decreasing $\beta w_p$ values. However, the $w_p$ terms of the nanocomposites examined, except that of PP/2.5BA80 composite, did not differ significantly ($p = 0.05$); thus, the dissipative plastic work was not influenced by the nanofillers.

## Conclusions

PP-based composites were prepared by melt compounding and film blowing techniques, using both untreated and surface-treated BA nanoparticles up to filler contents of 10 wt%, in order to assess the role of filler content and surface treatment on the thermal, mechanical and rheological properties of the resulting composites. The addition of surface-treated nanoparticles resulted in a better dispersion of the filler within the matrix, as confirmed by SEM observation. BA acted as a weak nucleating agent, producing a slight increase of the crystallization peak temperature. The melt viscosity of nanocomposites remained unaltered or decreased by the incorporation of nanofiller, at low contents (2.5 and 5 wt%), while it slightly increased at higher nanofiller contents (10 wt%). BA incorporation enhanced the resistance to thermal degradation of the PP matrix.

The mechanical properties of all samples were characterized by tensile, creep, DMTA and mode I-type fracture tests. The results of tensile tests indicated that the nanoparticles can stiffen PP even at a low filler content, especially in the case of treated BA, without a significant loss in ductility. Increasing stiffening was, however, accompanied with decreasing yield stress and elongation-at-yield.

Creep tests showed that creep compliance was remarkably reduced by nanofiller incorporation. Storage and loss moduli were enhanced in all the nanocomposites, demonstrating the reinforcing effect of the BA particles.

Finally, the toughness of the material, evaluated through EWF approach, showed an improvement, as indicated by a rise in the specific EWF values due to BA incorporation, with a decline occurring at higher filler contents because of nanofiller agglomeration.

### Funding

This research received no specific grant from any funding agency in the public, commercial, or not-for-profit sectors.

### Acknowledgements

This work was performed in the framework of a bilateral cooperation agreement between Italy and Hungary (HU11MO8-TET-10-1-2011-0218). The authors greatly acknowledge Professor Riccardo Ceccato of the Department of Industrial Engineering of the University of Trento for his kind assistance with the XRD analyses and rheological measurements.

### References

1. Dorigato A, Pegoretti A and Penati A. Linear low-density polyethylene/silica micro- and nanocomposites: dynamic rheological measurements and modelling. *Express Polym Lett* 2010; 4: 115–129.
2. Sengupta R, Bhattacharya M, Bandyopadhyay S, et al. A review on the mechanical and electrical properties of graphite and modified graphite reinforced polymer composites. *Prog Polym Sci* 2011; 36: 638–670.
3. Fu S, Feng X, Lauke B, et al. Effects of particle size, particle/matrix interface adhesion and particle loading on mechanical properties of particulate–polymer composites. *Compos Part B: Eng* 2008; 39: 933–961.
4. Paul DR and Robeson LM. Polymer nanotechnology: nanocomposites. *Polymer* 2008; 49: 3187–3204.
5. Gupta RK, Kennel E and Kim K-J. *Polymer nanocomposites handbook*. Boca Raton, FL: CRC Press, 2010.
6. Rong MZ, Zhang MQ, Pan SL, et al. Analysis of the interfacial interactions in polypropylene/silica nanocomposites. *Polym Int* 2004; 53: 176–183.
7. Dorigato A, Dzenis Y and Pegoretti A. Filler aggregation as a reinforcement mechanism in polymer nanocomposites. *Mech Mater* 2013; 61: 79–90.
8. Karger-Kocsis J. *Polypropylene: an A-Z reference*. Dordrecht, The Netherlands: Kluwer Publishers, 1999.
9. Ma P-C, Siddiqui NA, Marom G, et al. Dispersion and functionalization of carbon nanotubes for polymer-based nanocomposites: a review. *Compos Part A: Appl Sci Manufac* 2010; 41: 1345–1367.
10. Wu J, Xiang F, Han L, et al. Effects of carbon nanotubes on glass transition and crystallization behaviors in immiscible polystyrene/polypropylene blends. *Polym Eng Sci* 2011; 51: 585–591.
11. Kuriger RJ, Alam MK, Anderson DP, et al. Processing and characterization of aligned vapor grown carbon fiber reinforced polypropylene. *Compos Part A: Appl Sci Manufac* 2002; 33(1): 53–62.
12. Ardanuy M and Velasco JI. Mg–Al layered double hydroxide nanoparticles. *Appl Clay Sci* 2011; 51: 341–347.
13. Olewnik E, Garman K and Czerwiński W. Thermal properties of new composites based on nanoclay, polyethylene and polypropylene. *J Therm Anal Calorim* 2010; 101: 323–329.

14. Perrinsarazin F, Tonthat M, Bureau M, et al. Micro- and nano-structure in polypropylene/clay nanocomposites. *Polymer* 2005; 46: 11624–11634.
15. Kalaitzidou K, Fukushima H and Drzal LT. A new compounding method for exfoliated graphite–polypropylene nanocomposites with enhanced flexural properties and lower percolation threshold. *Compos Sci Technol* 2007; 67: 2045–2051.
16. Kalaitzidou K, Fukushima H and Drzal LT. Multifunctional polypropylene composites produced by incorporation of exfoliated graphite nanoplatelets. *Carbon* 2007; 45: 1446–1452.
17. Li M and Wu Z. A review of intercalation composite phase change material: preparation, structure and properties. *Renew Sustain Environ Rev* 2012; 16: 2094–2101.
18. Pedrazzoli D and Pegoretti A. Silica nanoparticles as coupling agents for polypropylene/glass composites. *Compos Sci Technol* 2013; 76: 77–83.
19. Karamipour S, Ebadi-Dehaghani H, Ashouri D, et al. Effect of nano-CaCO3 on rheological and dynamic mechanical properties of polypropylene: experiments and models. *Polym Test* 2011; 30: 110–117.
20. Wang Y, Shen H, Li G, et al. Crystallization and melting behavior of PP/CaCO3 nanocomposites during thermo-oxidative degradation. *J Therm Anal Calorim* 2010; 100: 999–1008.
21. Ogunniran ES, Sadiku R, Sinha RS, et al. Effect of boehmite alumina nanofiller incorporation on the morphology and thermal properties of functionalized poly(propylene)/polyamide 12 blends. *Macromol Mat Eng* 2012; 297: 237–248.
22. Özdilek C, Norder B and Picken SJ. A study of the thermo-mechanical behavior of boehmite-polyamide-6 nanocomposites. *Thermochim Acta* 2008; 472: 31–37.
23. Streller RC, Thomann R, Torno O, et al. Isotactic poly(propylene) nanocomposites based upon boehmite nanofillers. *Macromol Mat Eng* 2008; 293: 218–227.
24. Khumalo VM, Karger-Kocsis J and Thomann R. Polyethylene/synthetic boehmite alumina nanocomposites: structure, thermal and rheological properties. *Express Polym Lett* 2010; 4: 264–274.
25. Khumalo VM, Karger-Kocsis J and Thomann R. Polyethylene/synthetic boehmite alumina nanocomposites: structure, mechanical, and perforation impact properties. *J Mat Sci* 2010; 46: 422–428.
26. Halbach TS and Mülhaupt R. Boehmite-based polyethylene nanocomposites prepared by in-situ polymerization. *Polymer* 2008; 49: 867–876.
27. Halbach TS, Thomann Y and Mülhaupt R. Boehmite nanorod-reinforced-polyethylenes and ethylene/1-octene thermoplastic elastomer nanocomposites prepared byin situ olefin polymerization and melt compounding. *J Polym Sci Part A* 2008; 46: 2755–2765.
28. Özdilek C, Kazimierczak K and Picken SJ. Preparation and characterization of titanate-modified boehmite–polyamide-6 nanocomposites. *Polymer* 2005; 46: 6025–6034.
29. Tuba F, Khumalo VM and Karger-Kocsis J. Essential work of fracture of poly(ε-caprolactone)/boehmite alumina nanocomposites: effect of surface coating. *J Appl Polym Sci* 2013; 129(5): 2950–2958.
30. Zhang J, Ji Q, Zhang P, et al. Thermal stability and flame-retardancy mechanism of poly(ethylene terephthalate)/boehmite nanocomposites. *Polym Degrad Stabil* 2010; 95: 1211–1218.
31. Adhikari R, Brostow W, Datashvili T, et al. Effect of surfactant treated boehmite nanoparticles on properties of block copolymers. *Mat Res* 2012; 16: 19–24.
32. Hosseinpour D, Guthrie JT, Berg JC, et al. The effect of interfacial interaction contribution to the mechanical properties of automotive topcoats. *Prog Org Coat* 2005; 54: 182–187.
33. Bárány T, Czigány T and Karger-Kocsis J. Application of the essential work of fracture (EWF) concept for polymers, related blends and composites: a review. *Prog Polym Sci* 2010; 35: 1257–1287.
34. Mouzakis DE, Papanicolaou GC, Giannadakis K, et al. On the toughness response of iPP and sPP/MWNT nanocomposites. *Strain* 2013; 49: 348–353.
35. James E. *Polymer data handbook*. New York: Oxford University Press, 1999.
36. Banik K, Karger-Kocsis J and Abraham T. Flexural creep of all-polypropylene composites: model analysis. *Polym Eng Sci* 2008; 48: 941–948.
37. Tuba F, Oláh L and Nagy P. On the valid ligament range of specimens for the essential work of fracture method: the inconsequence of stress criteria. *Eng Fract Mech* 2013; 99: 349–355.
38. Tuba F, Oláh L and Nagy P. The role of ultimate elongation in the determination of valid ligament range of essential work of fracture tests. *J Mat Sci* 2012; 47: 2228–2233.
39. Cotterell B, Pardoen T and Atkins AG. Measuring toughness and the cohesive stress-displacement relationship by the essential work of fracture concept. *Eng Fract Mech* 2005; 72: 827–848.
40. Brostow W, Datashvili T, Huang B, et al. Tensile properties of LDPE + boehmite composites. *Polym Compos* 2009; 30: 760–767.
41. Pedrazzoli D, Ceccato R, Karger-Kocsis J, et al. Viscoelastic behaviour and fracture toughness of linear-low-density polyethylene reinforced with synthetic boehmite alumina nanoparticles. *Express Polym Lett* 2013; 7(8): 652–666.
42. Azároff LV. *Elements of X-ray crystallography*. Chapter 9. New York: McGraw-Hill Education, 1968.
43. Blaszczak P, Brostow W, Datashvili T, et al. Rheology of low-density polyethylene + boehmite composites. *Polym Compos* 2010; 31: 1909–1913.
44. Bocchini S, Morlat-Thérias S, Gardette J-L, et al. Influence of nanodispersed boehmite on polypropylene photooxidation. *Polym Degrad Stabil* 2007; 92: 1847–1856.
45. Kolarik J and Pegoretti A. Non-linear tensile creep of polypropylene: time-strain superposition and creep prediction. *Polymer* 2006; 47: 346–356.
46. Prashantha K. Processing and characterization of halloysite nanotubes filled polypropylene nanocomposites based on a masterbatch route: effect of halloysites treatment on structural and mechanical properties. *Express Polym Lett* 2011; 5: 295–307.

47. Williams JG and Rink M. The standardisation of the EWF test. *Eng Fract Mech* 2007; 74: 1009–1017.
48. Tuba F, Oláh L and Nagy P. Essential work of fracture study of polymers: a novel criterion for the validation of tested ligament range. *J Mat Sci* 2011; 46: 7901–7904.
49. Pegoretti A, Castellani L, Franchini L, et al. On the essential work of fracture of linear low-density-polyethylene. I. Precision of the testing method. *Eng Fract Mech* 2009; 76: 2788–2798.
50. Arkhireyeva A and Hashemi S. Combined effect of temperature and thickness on work of fracture parameters of unplasticized PVC film. *Polym Engin Sci* 2002; 42: 504–518.